Proceedings of the ASME 2021 Conference on Smart Materials, Adaptive Structures and Intelligent Systems
SMASIS2021
September 14-15, 2021, Virtual, Online

SMASIS2021-68183

DESIGN OF PENNATE TOPOLOGY FLUIDIC ARTIFICIAL MUSCLE BUNDLES UNDER SPATIAL CONSTRAINTS

Emily Duan
North Carolina State University
Raleigh, NC

Matthew Bryant
North Carolina State University
Raleigh, NC

ABSTRACT

In this paper, we investigate the design of pennate topology fluidic artificial muscle bundles under spatial and operating constraints. Soft fluidic actuators are of great interest to roboticists and engineers due to their potential for inherent compliance and safe human-robot interaction. McKibben fluidic artificial muscles (FAMs) are soft fluidic actuators that are especially attractive due to their high force-to-weight ratio, inherent flexibility, relatively inexpensive construction, and muscle-like force-contraction behavior. Observations of natural muscles of equivalent cross-sectional area have indicated that muscles with a pennate fiber configuration can achieve higher output forces as compared to the parallel configuration due to larger physiological cross-sectional area (PCSA). However, this is not universally true because the contraction and rotation behavior of individual actuator units (fibers) are both key factors contributing to situations where bipennate muscle configurations are advantageous as compared to parallel muscle configurations. This paper analytically explores a design case for pennate topology artificial muscle bundles that maximize fiber radius. The findings can provide insights on optimizing artificial muscle topologies under spatial constraints. Furthermore, the study can be extended to evaluate muscle topology implications on work capacity and efficiency for tracking a desired dynamic motion.

Keywords: biomimetic, pennate, soft actuators, fluidic artificial muscles, muscle topology

1. INTRODUCTION

The design of actuators plays a critical role in enabling the interaction of mechatronic systems and the physical world. Roboticists and engineers have drawn inspiration from the unique characteristics of biological muscles to develop actuators capable of safe human-robot interaction. Study of neuromuscular physiology and anatomy has shown that a single biological muscle tissue consists of many motor units. This design has been identified as cellular architecture and applied to actuator design such that a singular actuator consists of a collection of small actuator units [1]. Hierarchical actuation relies on this cellular architecture to extend the total actuator performance such that it increases functionality [2]. Cellular piezoelectric actuators [1], different levels of whiffletree actuators [2], series-parallel elastic actuators [3], and bioinspired orderly recruitment [4] have all demonstrated the practicality of this actuation strategy. This muscle-inspired hierarchy has led to the development of linear actuator bundles capable of mimicking orderly recruitment and thus improves efficiency through minimizing energy consumption in the smallest required actuator unit [4,5]. Recent studies have explored the parallel and pennate arrangement actuator bundle configurations. The parallel arrangement orients the longitudinal axis of individual actuators parallel to the bundle actuator line of motion. On the other hand, the pennate arrangement configures the longitudinal axis of individual actuators at an angle to the bundle actuator line of motion. Several studies have highlighted biological advantages of this pennate muscle topology as well as identified the effects of fiber pennation angle on speed of contraction, damping of impact disturbances, and aging [6-11]. Additionally, this muscle topology demonstrates the ability to passively change effective gear ratio since the muscle force and displacement are coupled with the fiber force and displacement. Several pennate actuator studies identified this variable gearing attribute and led to the development of a constitutive model for pennate actuators [9-11]. Furthermore, pennate actuator bundles have also been categorized as variable stiffness actuators, which are highly attractive for their potential in energy storage and safety in human-interaction [12]. McKibben fluidic artificial muscles (FAMs) are especially suitable for this application due to their muscle-like actuation behavior, inexpensive construction, inherent flexibility, and high force-to-weight ratio. Although previous pennate McKibben bundle case studies have provided insight into how fibers (individual McKibben actuator units) should be arranged and what parameters should be varied, there

has yet to be a unified approach to optimal fiber parameter design.

This paper explores the modeling, design, and analysis of a bio-inspired pennate topology fluidic artificial muscle actuator under spatial constraints. This analytical model has strengthened the understanding of fiber behavior during muscle contraction. A modified McKibben actuator bundle analytical model was used to further the understanding of the mechanical and performance implications of pennate topological configuration in fluidic artificial muscles.

2. METHODS

2.1 Design Case

In this configuration study, an entire actuator consists of multiple McKibben FAMs, where individual FAMs are referred to as "fibers" and the complete actuator is referred to as a "muscle". The design case considered in this study seeks to determine the fiber parameters, spacing, and number such that the fiber radius is maximized while constraining the muscle to remain within a prescribed bounding box spatial envelope throughout actuation. The fiber parameters of interest are fiber radius, fiber length, and the number of fibers that can be packed inside the bounding volume.

2.2 Muscle/System Configurations

Parallel and pennate configurations are the two topologies considered in this analysis. The fibers are oriented parallel to the muscle line of motion in the parallel configuration while the fibers are arranged at an angle to the muscle line of motion in the pennate configuration. A critical difference between the parallel and pennate configuration is the behavior of the individual fibers. The fibers in a parallel configuration are only subject to axial contraction when the muscle is activated. On the other hand, the fibers in a pennate configuration will not only axially contract but also rotate when the muscle is activated.

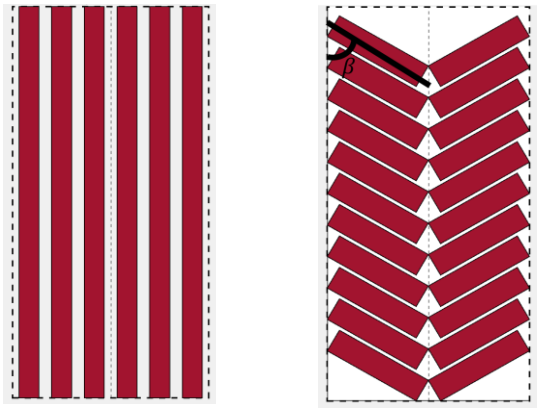

a) parallel configuration (b) bipennate configuration

FIGURE 1: VISUAL REPRESENTATION OF PARALLEL AND BIPENNATE MUSCLE TOPOLOGY

In this analysis, each muscle configuration considered is a single layer two-dimensional array of fibers. The initial braid angle α_i is the same for all fibers. The fibers in the bipennate configuration are symmetrically arranged.

Figure 1 is a visual representation of the two muscle topologies under consideration. Figure 1(a) illustrates the parallel fiber configuration and Figure 1(b) is the bipennate fiber configuration. The fibers are represented in the illustration as red rectangles due to the 2D projection of the circular cross section. The black dashed lines around the exterior indicate the length and width dimensions of a bounding box that surrounds the actuator bundle. The dimensions of this bounding box are defined such that all portions of the bundle remain fully inside the bounding box during inflation and contraction of the actuator fibers. The black dotted centerline is the muscle axis of motion. The β shown in Figure 1 (b) indicates the fiber pennation angle or the angle at which the fiber is orientated with respect to the muscle line of motion. It is important to note that an initial pennation angle of 0° in a pennate configuration is equivalent to fibers in a parallel configuration.

The boundary conditions are such that one end of each fiber is pinned to a rigid carriage subject to only vertical translational motion along the vertical dashed line during contraction and the other end is pinned to a rigid external frame.

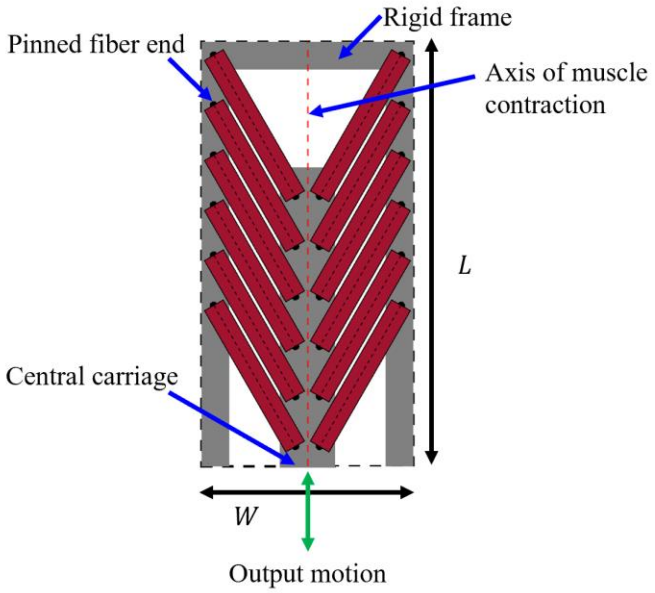

FIGURE 2: VISUAL REPRESENTATION OF FIBER END BOUNDARY CONDITIONS OF BIPENNATE CONFIGURATION

Figure 2 illustrates the fiber boundary conditions of the bipennate configuration considered in this study. The black half-circle marker indicates the fiber end has a pinned boundary condition. It also identifies the dimension parameters of the

prescribed bounding box. The illustrations in Figure 2 are in the planar view so the depth dimension is not indicated on the figure.

Table 1: System parameters

Parameter	Value
α_i	30°
L	30.48 cm(12 in)
W	15.24 cm (6 in)
D	2.54 cm (1 in)

Table 1 shows the initial braid angle of the mesh for each fiber as well as the prescribed bounding box parameter dimensions.

2.3 Modeling

This section details a model developed to determine the optimal set of fiber parameters based on the initial pennation angle of the fiber for the specified design objective. The initial pennation angle can be used to provide insight on the fiber behavior during muscle contraction. The fibers in the configuration can be contraction-limited, rotation-limited or both at the maximum contraction condition of the muscle. If the fibers are contraction-limited, it indicates the fibers are not capable of reaching full rotation but will reach full contraction. On the contrary, if the fibers are rotation-limited, it indicates the fibers are not capable of reaching full contraction but will reach full rotation. If the fiber is both contraction and rotation-limited, it indicates that the fiber will reach full contraction and full rotation simultaneously.

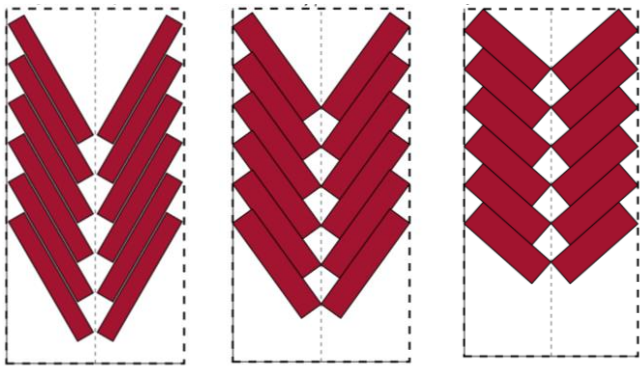

(a) $\varepsilon_m = 0$ (b) $\varepsilon_m = \frac{\varepsilon_{free}}{2}$ (c) $\varepsilon_m = \varepsilon_{free}$

FIGURE 3: VISUAL REPRESENTATION OF CONTRACTION-LIMITED FIBERS DURING FREE MUSCLE CONTRACTION

Figure 3 is a visual representation of contraction-limited fiber behavior during free muscle contraction of a bipennate configuration. Each image is a snapshot of the fiber dimension and orientation at different stages of free muscle contraction. Figure 3(a) shows the initial fiber configuration prior to any muscle contraction or at zero muscle strain ε_m. Figure 3(b) shows some fiber contraction and rotation occurring as the muscle is contracting, where muscle strain has reached half of muscle free strain. Figure 3(c) shows that the fibers have fully contracted at free muscle contraction but not fully rotated at muscle free strain. Therefore, the fibers in this muscle configuration are contraction-limited. [13]

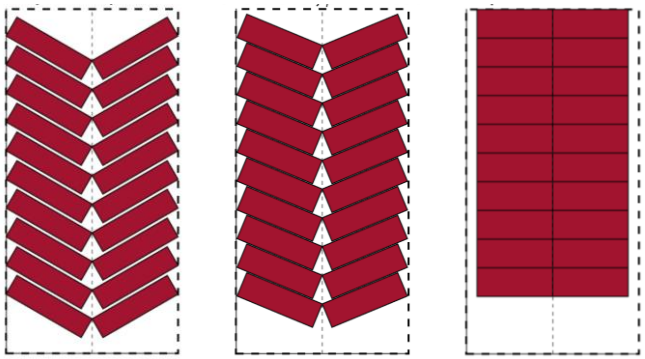

(a) $\varepsilon_m = 0$ (b) $\varepsilon_m = \frac{\varepsilon_{free}}{2}$ (c) $\varepsilon_m = \varepsilon_{free}$

FIGURE 4: SNAPSHOTS OF ROTATION-LIMITED FIBERS DURING FREE MUSCLE CONTRACTION

Figure 4 is a visual representation of rotation-limited fiber behavior during free muscle contraction of a bipennate configuration. Like Figure 3, each image is a snapshot of the fiber dimension and orientation at different stages of free muscle contraction. Figure 4(a) shows the initial fiber configuration prior to any muscle contraction. Figure 4(b) shows some fiber contraction and rotation occurring as the muscle is contracting. Figure 4(c) shows that the fibers have fully rotated at free muscle contraction. It can be difficult to determine if the fibers at free muscle contraction have also fully contracted in this visual representation. However, the following mathematical analysis can indicate if the fibers in the muscle configuration are contraction-limited, rotation-limited or both. We will consider the fibers as idealized McKibben actuators.

The free-contraction pennation angle can be expressed as

$$\beta_{free} = sin^{-1}\left(\frac{sin(\beta_i)\cos(\alpha_i)}{\cos(54.7°)}\right) \quad (1)$$

where β_{free} is the pennation angle at free muscle contraction, β_i is the fiber initial pennation angle, and α_i is the initial braid angle. If $0° \leq \beta_{free} < 90°$, fibers cannot fully rotate at free muscle contraction. Consequently, the braid angle at free muscle contraction, α_{free}, is 54.7°, which is the maximum possible braid angle, α_{max}, for an ideal McKibben muscle [13]. When $\alpha_{free} = \alpha_{max}$ and $\beta_{free} < 90°$, the fibers in that configuration are contraction-limited. If $\beta_{free} = 90°$, the fibers can fully rotate at free muscle contraction. However, it does not necessarily indicate the fibers are rotation-limited. The braid angle at free muscle contraction can be computed in (2) to determine if the fibers are solely rotation-limited or both contraction and rotation-limited.

$$\alpha_{free} = \cos^{-1}(sin(\beta_i)\cos(\alpha_i)) \quad (2)$$

If $\beta_{free} = 90°$ and $\alpha_{free} = \alpha_{max}$, the fibers are both contraction and rotation-limited. However, if $\beta_{free} = 90°$ and $\alpha_{free} < \alpha_{max}$, the fibers in that configuration are purely rotation limited.

Based on a well-established understanding of ideal McKibben muscle behavior during contraction, relationships can be derived to understand how fiber radius and fiber length change with braid angle. [13]

$$\frac{r_f}{r_{f,i}} = \frac{\sin(\alpha)}{\sin(\alpha_i)} \tag{3}$$

$$\frac{l_f}{l_{f,i}} = \frac{\cos(\alpha)}{\cos(\alpha_i)} \tag{4}$$

$r_f, l_f,$ and α are the instantaneous fiber radius, fiber length and braid angle, respectively.

For this study, relationships between fiber parameters and the bounding box constraint can be formulated to ensure that the fibers remain inside the bounding box during muscle contraction [12]:

$$2r_f \cos(\beta_f) + l_f \sin(\beta_f) \leq \frac{W}{2} \tag{5}$$

$$(\frac{n_w}{2} - 1)\frac{2r_f}{\cos(\beta_f)} + (2r_f \cos(\beta_f) + l_f \sin(\beta_f)) \leq \frac{W}{2} \tag{6}$$

$$\left(\frac{n_l}{2} - 1\right)\frac{2r_f}{\sin(\beta_f)} + 2r_f \sin(\beta_f) + l_f \cos(\beta_f) \leq L \tag{7}$$

where n_w is the number of fibers that can fit along the prescribed width dimension of the bounding box W and n_l is the number of fibers that can fit along the prescribed length dimension of the bounding box L. Although these constraints can provide insight on feasible fiber parameters, additional work is needed to determine the optimal set of fiber parameters for each design case.

To maximize fiber radius, a constraint is applied to the fiber radius at free muscle contraction r_{free} due to the depth dimension of the bounding box as shown in (3).

$$r_{free} = \frac{D}{2} \tag{8}$$

D is the depth dimension of the bounding box. This expression bounds the fiber radius parameter such that the fiber remains inside the bounding box during muscle contraction. The initial fiber radius $r_{f,i}$ can be derived from this constraint.

For a parallel configuration, the fibers only contract axially during muscle contraction. Therefore, the fibers in a parallel configuration are always contraction-limited. The initial fiber length and the number of fibers in the parallel configuration are bounded by the length and width dimensions of the bounding box, respectively. The initial fiber length $l_{f,i}$ is maximized such that it is equivalent to the length of the bounding box.

$$l_{f,i} = L \tag{9}$$

Fibers in the parallel configuration are arranged along the width dimension of the bounding box. Therefore, the maximum number of fibers n that can fit inside the bounding box in the parallel configuration can be computed from the inequality in (7).

$$n \leq \frac{W}{2r_{free}} \tag{10}$$

n must also be a positive non-zeros integer. In the parallel configuration, $n = n_w$ and $n_l = 1$.

For bipennate configurations, the fiber length and the maximum number of fibers that fit in the bounding box depend on the fiber behavior. Although the constraints can provide insight on the fiber parameters, $l_{f,i}$ and n are coupled and will depend on the minimum fiber clearance required to enable the fibers to fully contract, rotate or both. An initial fiber length can be estimated from the following relationship.

$$l_{f,i} = \max\left(\frac{L - max(r_f\, sin(\beta_f)) - r_f\, sin(\beta_f)}{\frac{cos(\alpha)}{cos(\alpha_i)}\cos(\beta_f)}\right) \tag{11}$$

This relationship depends on the minimum vertical fiber clearance of the top-most pair of fibers, $max(r_f\, sin(\beta_f))$. Assuming that at least one pair of fibers can fit along the width dimension of the bounding box and $n_w = 2$, this estimated initial fiber length must satisfy inequality (6). If this estimated initial fiber length satisfies inequality (6) during contraction, then this guess is valid. However, this does not necessarily indicate that a single pair of fibers is the maximum number of fibers that can fit along the width dimension of the bounding box or $n_w = 2$. The exact n_w and n_l should be determined using inequality (6) and inequality (7) respectively with a suitable set of fiber dimensions. If this estimated initial fiber length violates inequality (6) during contraction, the estimated initial fiber length is no longer valid and must be recomputed with the assumption that only one pair of fibers can fit along the width dimension of the bounding box and $n_w = 2$ as shown in the relationship below.

$$l_{f,i} = \min\left(\frac{\frac{W}{2} - 2r_f\, cos(\beta_f)}{\frac{cos(\alpha)}{cos(\alpha_i)} sin(\beta_f)}\right) \tag{12}$$

Thus, n_l can be found from inequality (7) with the minimum vertical clearance required between the fibers, $\max\left(\frac{2r_f}{\sin(\beta_f)}\right)$. If $n_w > n_l$, the fibers will be laterally arranged. If $n_w < n_l$, the fibers will be centrally arranged. If $n_w = n_l$, the fibers can be arbitrarily arranged. It is important to note that both n_w and n_l must be even and positive non-zero integers to maintain the bipennate configuration. A visual representation of laterally attached and centrally attached fibers is shown in Figure 5.

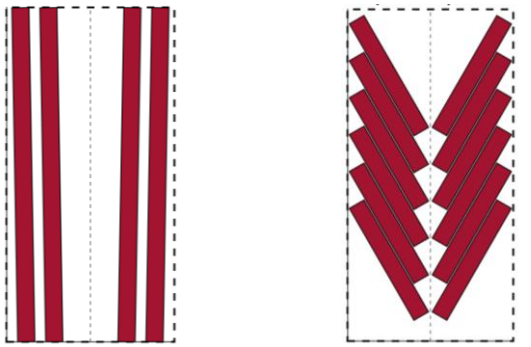

(a) Laterally attached (b) Centrally attached

FIGURE 5: VISUAL REPRESENTATION OF LATERAL AND CENTRALLY ATTACHED FIBERS

3. RESULTS AND DISCUSSION

An optimal set of fiber parameters were found using the analytical model presented and the system parameters shown in Table 1.

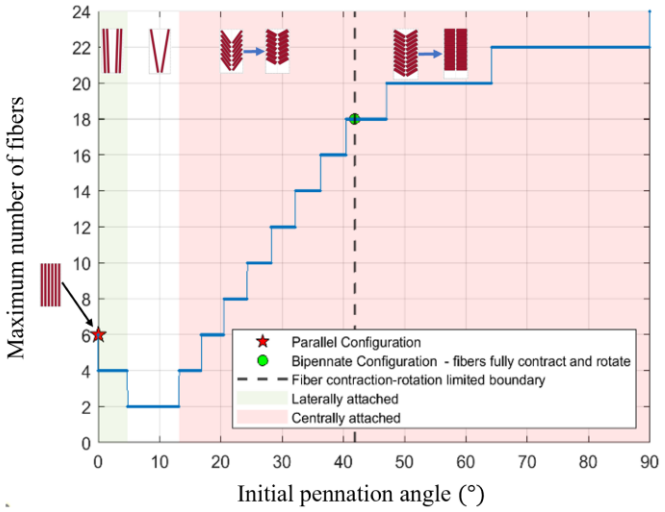

(a) Maximum number of fibers that can fit inside prescribed boundary box

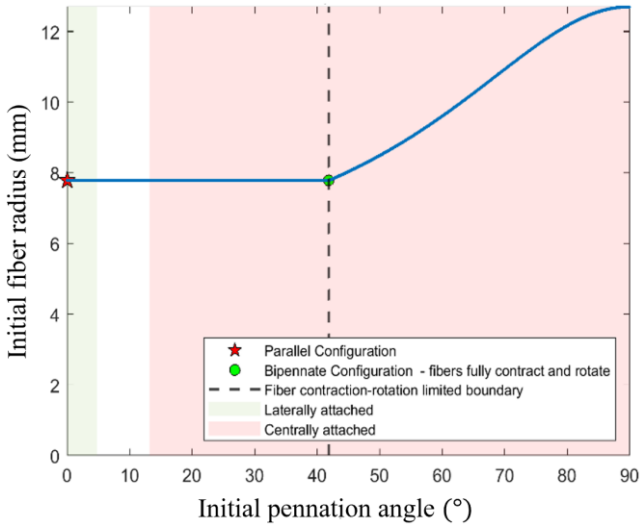

(b) Initial fiber radius with respect to initial pennation angle

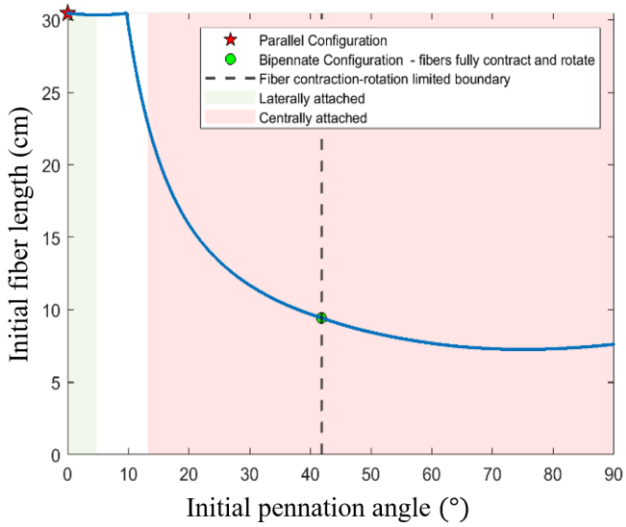

(c) Initial fiber length with respect to initial pennation angle

FIGURE 6: OPTIMAL SET OF FIBER PARAMETERS THAT MAXIMIZE FIBER RADIUS

Figure 6 shows the optimal set of fiber parameters as a function of initial pennation angle such that fiber radius is maximized. The red star marker indicates the parallel configuration while the green circle marker represents the bipennate configuration where fibers can both fully contract and rotate. The black vertical dashed line indicates the fiber contraction-/rotation-limited boundary line for bipennate configurations. Regions shaded in light green indicate configurations where fibers are laterally attached while regions shaded in pink are configurations where fibers are centrally attached. The unshaded region indicates bipennate fibers associated with those initial pennation angles are not restricted to lateral or central attachment.

The discontinuities seen in the curve for the plot shown in Figure 6(a) correspond to the addition of a pair of fibers to the muscle configuration. The change in number of fibers as fiber initial pennation angles increases shows that muscles with a small fiber initial pennation angle must be laterally attached, while fibers with a larger fiber initial pennation angles must be centrally attached. The thumbnail pointing to the red star marker illustrates the parallel configuration while the thumbnail found in the light green region illustrates a bipennate muscle with laterally attached fibers. The thumbnail in the white region show only one pair of fibers can fit in these configurations and thus the fibers can be arbitrarily attached. The illustration found in the pink region to the left of the vertical dashed line depicts the fibers in these configurations to be contraction-limited and centrally attached. The graphic to the right of the vertical dashed line indicates the fibers in these configurations to be rotation-limited and centrally attached.

Figure 6 (b) illustrates the initial fiber radius with respect to fiber initial pennation angle for maximizing fiber radius. For fiber contraction-limited configurations, $(0° \leq \beta_i \leq 41.86°)$, the initial fiber radius is maximized such that the fibers can fully contract. On the other hand, the rotation-limited configurations $(\beta_i > 41.86°)$ are not capable of fully contracting, so the initial fiber radius can be larger than that of the fiber contraction-limited configurations. Figure 6(c) illustrates the initial fiber length with respect to fiber initial pennation angle. A maximum initial fiber length exists at the parallel configuration since the fibers are only bounded by the length dimension of the bounded box. Although it is hard to discern, bipennate configurations with small fiber initial pennation angles can have an initial fiber length larger than the fibers in a parallel configuration since the fibers are arranged at an angle. However, at some fiber initial pennation angle, the fiber length is forced to decrease to ensure the fibers remain inside the prescribed bounding box. The nonlinear behavior observed in the fiber length as fiber initial pennation angle increases for fiber contraction-limited configurations is a result of the fiber contraction and rotation behavior.

Using the optimal set of fiber parameters for maximizing fiber radius, we next consider how optimized muscle performance depends on initial pennation angle.

The maximum muscle contraction $\Delta l_{m,max}$ can be computed as the difference between initial muscle length $l_{m,i}$ and muscle length at free muscle contraction $l_{m,free}$.

$$\Delta l_{m,max} = l_{m,i} - l_{m,free} = l_{f,i}\cos(\beta_i) - l_{free}\cos(\beta_{free}) \qquad (13)$$

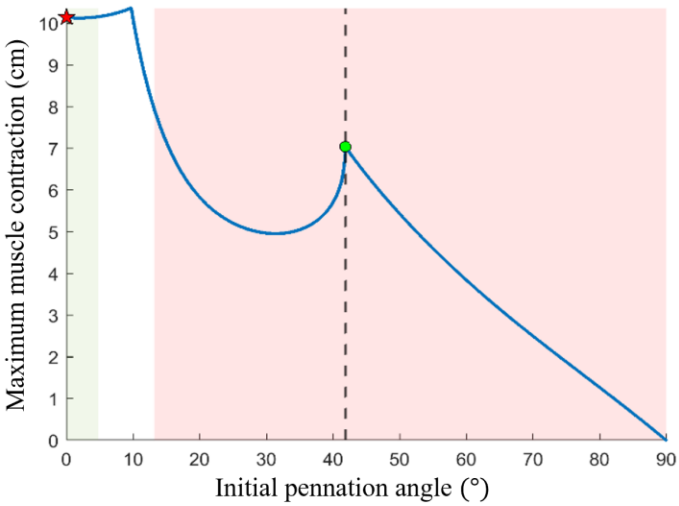

FIGURE 7: MAXIMUM MUSCLE CONTRACTION WITH RESPECT TO INITIAL PENNATION ANGLE

The maximum muscle contraction depends on both the fiber length and the pennation angle. Bipennate fibers are subject to contraction and rotation during muscle contraction, which explains the nonlinear behavior seen in the fiber contraction-limited configurations from Figure 7. Furthermore, a maximum muscle contraction peak observed at bipennate configurations with a small fiber initial pennation angle exceeds that of the parallel configuration. On the other hand, the maximum muscle contraction decreases significantly with initial pennation angle in fiber rotation-limited configurations. This is due to a shorter fiber length and limited fiber rotation during muscle contraction.

The modified nonlinear force-strain relationship represented by the ideal virtual work model for a pennate topology [11] is used to understand the muscle force behavior during free muscle contraction at different initial pennation angles. This relationship can provide insight on the force generation performance of the muscle.

$$F_m(\Delta l_m) = n\pi r_{f,i}^2 P(a(1-\varepsilon)^2 - b)\cos(\beta_f) \qquad (14)$$

$$\varepsilon = \frac{\Delta l_f}{l_{f,i}} \qquad a = \frac{3}{tan(\alpha_i)^2} \qquad b = \frac{1}{sin(\alpha_i)^2}$$

$F_m(\Delta l_m)$ is the muscle force with respect to muscle contraction, where P is the applied pressure, a and b are constants related to the initial braid angle. ε is the fiber strain and will vary based on fiber configuration and behavior.
For the parallel configuration,

$$\varepsilon = \frac{l_{f,i} - \dfrac{l_{f,i}\cos(\beta_i) - \Delta l_m}{\cos(\beta_i)}}{l_{f,i}} \qquad (15)$$

For the bipennate configurations,

$$\varepsilon = \frac{l_{f,i} - \dfrac{l_{f,i}\sin(\beta_i)}{\sin\left(\tan^{-1}\left(\dfrac{l_{f,i}\sin(\beta_i)}{l_{f,i}\cos(\beta_i) - \Delta l_m}\right)\right)}}{l_{f,i}} \tag{16}$$

Muscle blocked force $F_{m,block}$ can be derived from the modified nonlinear force-strain relationship to compare the maximum possible output force of different muscle configurations. The muscle blocked force is computed as the muscle force at zero strain. For this analysis, applied pressure P is held constant to accurately.

$$F_{m,block} = F_m(\Delta l_m)|_{\varepsilon=0} \tag{17}$$

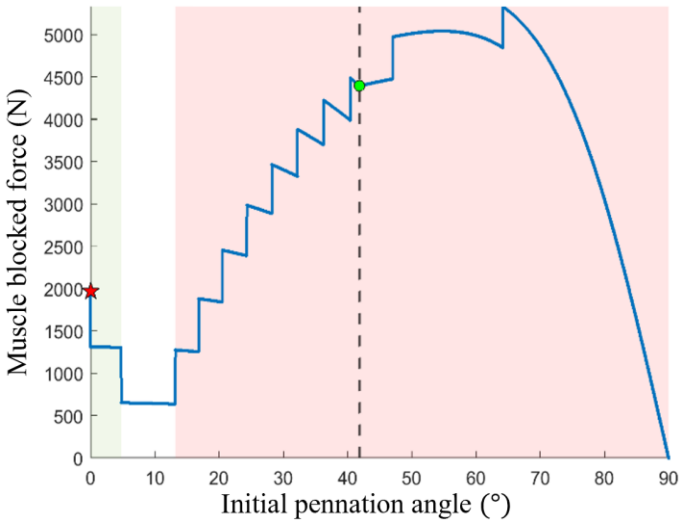

FIGURE 8: MUSCLE BLOCKED FORCE WITH RESPECT TO INITIAL PENNATION ANGLE

The muscle blocked force is evaluated with a constant applied pressure of 50 psi (344.74 kPa). Figure 8 shows the change in muscle blocked force as fiber initial pennation angle increases. The steps observed in the curve are associated with changes in the number of fibers in the muscle configuration as shown in Figure 6(a). This plot shows that muscles with a bipennate configuration are capable of outputting a muscle blocked force significantly larger than that of a parallel configuration. For fiber contraction-limited configurations, the muscle blocked force is driven by the number of fibers that can be packed in the prescribed bounding box. This is the case since the initial fiber radiuses are all the same for fiber contraction-limited configurations. In addition, fiber initial pennation angles are relatively small, which indicates most of the muscle output force is exerted along the same direction as the muscle line of motion. For fiber rotation-limited configurations, a nonlinear relationship exists between the muscle blocked force and fiber initial pennation angle due to a combination of factors. Both the number of fibers and initial fiber radius increases with increasing fiber initial pennation angle such that the maximum muscle blocked force is observed in a purely fiber rotation-limited configuration. However, the muscle blocked force decreases significantly for large fiber initial pennation angles. This is due to the amount of muscle output force exerted in the direction of muscle motion. At larger fiber initial pennation angles, less muscle output force is exerted in the direction of muscle contraction.

Maximum muscle free contraction in Figure 7 and muscle blocked force in Figure 8 provide insight to understand how muscle stiffness varies with fiber initial pennation angle. The muscle stiffness k_m can be computed from the muscle force behavior during free muscle contraction. In this analysis, applied pressure P is held constant for a fair comparison.

$$k_m = \frac{dF_m}{d\Delta l_m} \tag{18}$$

Muscle stiffness at blocked force $k_{m,block}$ can be extracted from the muscle force behavior.

$$k_{m,block} = k_m|_{\Delta l_m=0} \tag{19}$$

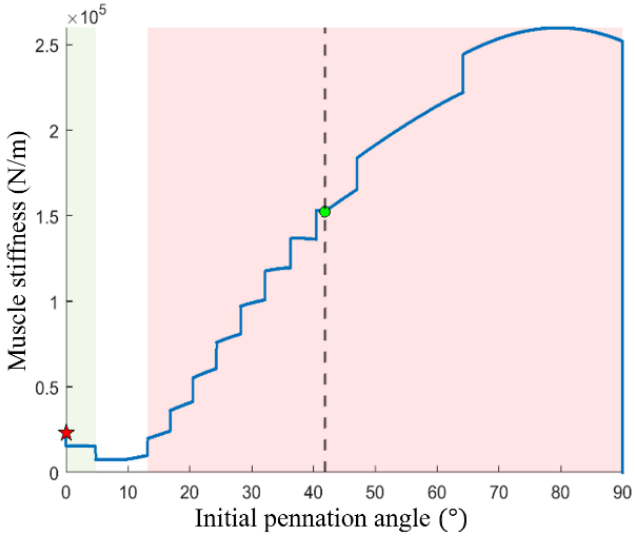

FIGURE 9: MUSCLE STIFFNESS AT BLOCKED FORCE WITH RESPECT TO INITIAL PENNATION ANGLE

Intuitively, a muscle configuration with a large fiber initial pennation angle is expected to have a smaller muscle stiffness as compared to the same muscle configuration but, with a small fiber initial pennation angle due to the rate of change of fiber length with respect to muscle deflection. However, in this study, bipennate muscles with large fiber initial pennation angles can pack in more fibers and the fiber radiuses are larger than that of muscle configurations with smaller fiber initial pennation angles. This results in muscles with large fiber initial pennation angles achieving higher muscle output forces and small muscle contraction, which contribute to an overall large muscle stiffness. Figure 9 shows the change in muscle stiffness at blocked force as fiber initial pennation angle increases. The steps

seen in the plot are associated with changes in the number of fibers in the muscle configuration. The muscle stiffness at blocked force significantly increases with increasing initial pennation angle of the fibers. This is primarily due to the number of fibers in the muscle configuration. Like muscle blocked force, the maximum muscle stiffness at blocked force is observed in the purely fiber-rotation-limited configuration. However, this purely fiber-rotation-limited configuration for maximum muscle stiffness is different from that for maximum muscle blocked force.

Isobaric work $W_{isobaric}$ can be evaluated from the understanding the muscle force behavior during contraction. In this analysis, applied pressure P is again held constant for a fair comparison.

$$W_{isobaric} = \int_{l_{m,i}}^{l_{m,free}} F_m dl_m \tag{20}$$

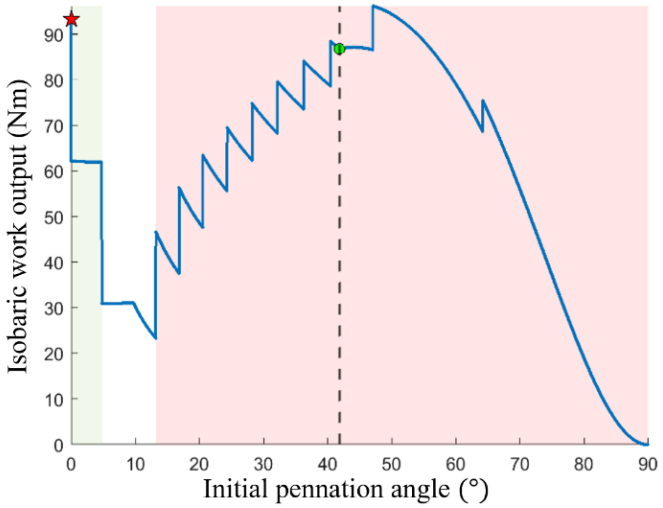

FIGURE 10: ISOBARIC WORK OUTPUT CAPACITY WITH RESPECT TO INITIAL PENNATION ANGLE

The isobaric pressure applied to all muscle configurations was $50\ psi$ ($344.74\ kPa$). Figure 10 illustrates the isobaric work output capacity varying with initial pennation angle. The steps in the plot are associated with changes in the number of fibers in the muscle configuration. Although the maximum isobaric work is hard to discern, there is a bipennate configuration such that with isobaric work output capacity that is slightly larger than that of the parallel configuration. The bipennate configuration with maximum isobaric work is purely fiber rotation-limited and differs from the bipennate configuration for maximum muscle blocked force and maximum muscle stiffness. This shows that bipennate muscles can be designed to achieve at least equivalent, even slightly more, work output under isobaric operation as compared to a muscle with parallel fibers.

Isotonic work output $W_{isotonic}$ can also be evaluated from the muscle force during muscle contraction.

$$W_{isotonic} = F_{load} \int_{l_{m,i}}^{l_{m,free}} dl_m \tag{21}$$

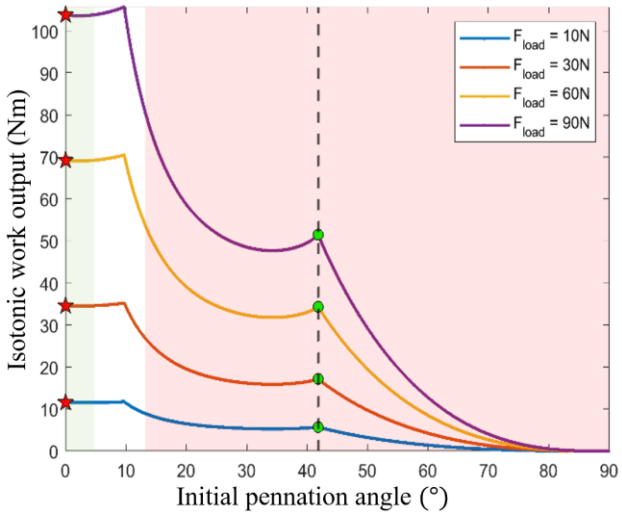

FIGURE 11: ISOTONIC WORK OUTPUT CAPACITY VS. INITIAL PENNATION ANGLE FOR DIFFERENT LOADS

Figure 11 shows the isotonic work output for 10N, 30N, 60N and 90N loads. The curves indicate that there is at least one bipennate configuration capable of achieving an isotonic work output larger than that of a parallel configuration. The results indicate the maximum isotonic work exists at the same fiber contraction-limited bipennate configuration regardless of load conditions.

3 CONCLUSIONS

In this paper, a parametric model was presented to understand design considerations for pennate topology artificial muscle bundles under spatial bounding constraints. This model gave insight to not only how the individual fibers would behave during contraction but also indicated different methods of fiber attachment. Comparisons between the bipennate and parallel topology under equal spatial bounding constraint indicate that the pennate topology provides opportunities for amplifying muscle contraction, muscle output force, and muscle stiffness, while maintain similar peak isobaric work output. Particularly, pennate topology can amplify maximum muscle contraction by approximately 2.2% and maximum muscle blocked force by approximately 2.7 times as compared to the parallel configuration. This clear tradeoff between muscle contraction and muscle output force aligns with the biomechanics of natural muscles as pennate muscles are located where maximum force and minimum motion is needed. The maximum muscle stiffness is approximately 11 times larger than that of the parallel configuration. The maximum isobaric work is approximately 3% greater than that of the parallel configuration. Maximum isotonic work is approximately 1.8% greater than that of the parallel configuration regardless of load applied. Further work will include other design cases and efficiency analysis as well as

experimental validation of different muscle topologies for tracking a desired dynamic motion.

ACKNOWLEDGEMENTS

This work was supported primarily by the Faculty Early Career Development Program (CAREER) of the National Science Foundation under NSF Award Number 1845203 and Program Manager Irina Dolinskaya. A NC Space Grant Graduate Research Fellowship also supported this research.

REFERENCES

[1] J. Ueda, J. A. Schultz, and H. H. Asada, "Structure of cellular actuators," *Cellular Actuators*, pp. 1–44, 2017.

[2] D. Huston, B. Esser, G. Spencer, D. Burns, and E. Kahn, "Hierarchical actuator systems," *Smart Structures and Materials 2005: Industrial and Commercial Applications of Smart Structures Technologies*, 2005.

[3] G. Mathijssen, D. Lefeber, and B. Vanderborght, "Variable Recruitment of Parallel Elastic Elements: Series–Parallel Elastic Actuators (SPEA) With Dephased Mutilated Gears," *IEEE/ASME Transactions on Mechatronics*, vol. 20, no. 2, pp. 594–602, 2015.

[4] M. Bryant, M. A. Meller, and E. Garcia, "Variable recruitment fluidic artificial muscles: modeling and experiments," *Smart Materials and Structures*, vol. 23, no. 7, p. 074009, 2014.

[5] M. Meller, J. Chipka, A. Volkov, M. Bryant, and E. Garcia, "Improving actuation efficiency through variable recruitment hydraulic McKibben muscles: modeling, orderly recruitment control, and experiments," *Bioinspiration & Biomimetics*, vol. 11, no. 6, p. 065004, 2016.

[6] E. Azizi, E. L. Brainerd, and T. J. Roberts, "Variable gearing in pennate muscles," *Proceedings of the National Academy of Sciences*, vol. 105, no. 5, pp. 1745–1750, 2008.

[7] N. C. Holt, N. Danos, T. J. Roberts, and E. Azizi, "Stuck in gear: age-related loss of variable gearing in skeletal muscle," *Journal of Experimental Biology*, vol. 219, no. 7, pp. 998–1003, 2016.

[8] E. Azizi and T. J. Roberts, "Geared up to stretch: pennate muscle behavior during active lengthening," *Journal of Experimental Biology*, vol. 217, no. 3, pp. 376–381, 2014.

[9] E. Azizi and T. J. Roberts, "Variable gearing in a biologically inspired pneumatic actuator array," *Bioinspiration & Biomimetics*, vol. 8, no. 2, p. 026002, 2013.

[10] S. Kianzad, M. Pandit, J. D. Lewis, A. R. Berlingeri, K. J. Haebler, and J. D. Madden, "Variable stiffness structure using nylon actuators arranged in a pennate muscle configuration," *Electroactive Polymer Actuators and Devices (EAPAD) 2015*, 2015.

[11] T. Jenkins and M. Bryant, "Pennate actuators: force, contraction and stiffness," *Bioinspiration & Biomimetics*, vol. 15, no. 4, p. 046005, 2020.

[12] T. E. Jenkins and M. Bryant, "Variable stiffness soft robotics using pennate muscle architecture," *Bioinspiration, Biomimetics, and Bioreplication IX*, 2019.

[13] B. Tondu and P. Lopez, "Modeling and control of McKibben artificial muscle robot actuators," *IEEE Control Systems*, vol. 20, no. 2, pp. 15–38, 2000.